Research Article | Vol. 27, No. 8 | 15 Apr 2019 | OPTICS EXPRESS 11037
Optics EXPRESS

Frequency-comb-based laser system producing stable optical beat pulses with picosecond durations suitable for high-precision multi-cycle terahertz-wave generation and rapid detection

D. N. SCHIMPF,[1,*] H. T. OLGUN,[1,2] A. KALAYDZHYAN,[1] Y. HUA,[1] N. H. MATLIS,[1] AND F. X. KÄRTNER[1,3]

[1]*Center for Free-Electron Laser Science, Deutsches Elektronen Synchrotron, Hamburg, 22607, Germany*
[2]*Helmholtz-Institute Jena, Fröbelstieg 3, 07743, Jena, Germany*
[3]*Department of Physics and The Hamburg Centre for Ultrafast Imaging, University of Hamburg, 22761, Germany*
[*]*damian.barre@desy.de*

Abstract: We generate temporally modulated optical pulses with a beat frequency of 255 GHz, a duration of 360 ps, and a repetition rate of 2 MHz. The temporal envelope, beat frequency, and repetition rate are computer-programmable. A frequency comb serves as a phase and frequency reference for the locking of two laser lines. The system enables beat frequencies that are adjustable in steps of the frequency comb's repetition rate and exhibit Hz-level precision and accuracy. We expect the optical beat pulses to be well suited for versatile multi-cycle terahertz-wave generation with controllable carrier-envelope phase. We demonstrate that the inherent synchronization of the frequency comb's ultra-short pulse train and the synthesized optical beat (or later the multi-cycle terahertz) pulses enables rapid and phase-sensitive sampling of such pulses.

1. Introduction

Terahertz waves offer capabilities unavailable through conventional RF or optical methods. For instance, terahertz waves have applications in remote sensing, high-resolution imaging for defense or bio-medical application as well as ultra-broadband directional wireless communication [1–3]. Novel terahertz applications also include compact electron acceleration [4–6]. To enable these unique applications, the field of terahertz photonics merges photonic technologies with microwave engineering [7,8]. Compared to traditional radio frequency (RF) bands, the advantages of operation at terahertz frequencies comprise smaller dimensions of corresponding system components, the potential use of higher accelerating fields and field gradients and the use of optical diagnostic techniques. However, the limited availability of adequate terahertz coherent sources and detection schemes imposes limitations on the utility of terahertz waves in applications.

In this contribution, we propose and demonstrate a frequency-comb-based laser source producing a phase-stable optical beat signal of which the envelope is a pulse with a picosecond durations. The pulse's shape, duration and repetition rate of the optical beat are computer-programmable by using a combination of optical amplitude modulator and an electronic arbitrary waveform generator. The optical beat signal, which is enveloped by this pulse, exhibit beat frequencies on THz-scale that can be set with Hz precision and accuracy. In principle, the beat frequency is adjustable from a few GHz up to multiple THz in steps of the frequency comb's repetition rate. Note, we refer to those temporally modulated optical

#360084 https://doi.org/10.1364/OE.27.011037
Journal © 2019 Received 13 Feb 2019; revised 15 Mar 2019; accepted 16 Mar 2019; published 4 Apr 2019

Optics EXPRESS

pulses as 'optical beat pulses' in the following, They are well suited for versatile multi-cycle terahertz wave generation. The pulse shaping enables tailoring of the resulting terahertz waveforms to the needs of applications.

Compared to recently demonstrated opto-electronic frequency comb generators [8,9], the main advantage of our system includes an inherent synchronization of the ultra-short pulse train of the laser frequency comb and the synthesized optical beat (or terahertz) pulses. The synchronization enables rapid and phase-sensitive detection of those synthesized pulses by using optical cross-correlation in the optical domain (or electro-optical sampling in the terahertz domain).

The paper is structured as follows: in section 2 we present the fundamentals and the design strategies of the laser system producing optical beat pulses with picosecond durations. Emphasis is placed on optimization of the optical beat pulse for terahertz generation, as well as the rapid detection of the terahertz waveforms. In section 3, we explain the experimental setup. The experimental results are shown in section 4. In section 5, we provide a conclusion and outlook.

2. Fundamentals and design of the laser system

2.1 Optical beats with beat frequencies exhibiting Hz-level precision and accuracy

Figure 1(a) illustrates the principle of the laser-based production of terahertz waves. Frequency conversion from the optical domain to the terahertz domain is achieved by the nonlinear optical effect of difference frequency generation (DFG). The laser output contains two spectrally distinct components (or lines), which are separated by the desired terahertz frequency. In a second-order nonlinear medium, this frequency difference is optically rectified to a corresponding terahertz frequency. So, the key to generation of terahertz waves with frequencies of high precision and high accuracy is a highly precise frequency difference between the two laser lines in the optical domain.

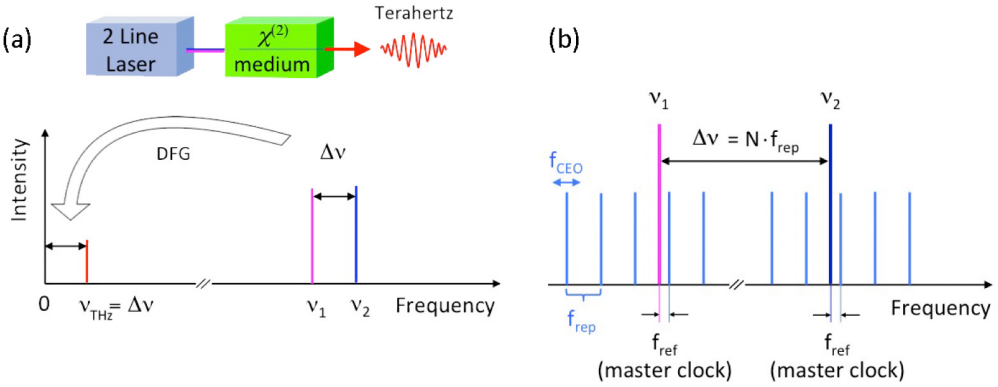

Fig. 1. (a): Laser-based generation of terahertz radiation using the nonlinear effect of difference frequency generation, (b) generation of a highly precise and accurate frequency difference between two single frequency lasers using a laser frequency comb.

There exist lasers that directly output multiple laser lines. Both continuous wave and pulsed operations of such lasers have been demonstrated [10,11]. However, the spectral profile of the gain medium and the filters, which are used for line selection, determine the frequency difference between the laser lines. This constraint imposes limitations on the available frequency differences and its precision. Also, the generation of two laser lines which each contain only a single frequency is challenging.

In this contribution, we generate a two-line output by using two single frequency lasers with respective center optical frequencies ν_1 and ν_2. The single frequency laser lines can be tuned in center wavelength, e.g., by using external cavity diode lasers. This approach has the

Optics EXPRESS

following benefits: first, the frequency difference between the two lines can be adjusted to obtain a desired frequency in the THz range. Second, both laser lines can be spectrally tuned to match the gain peak of subsequent booster amplifiers.

As shown in Fig. 1(b), the two laser lines are locked to the frequency comb of an ultra-short pulse laser, which provides a stabilized frequency difference and a common phase for both lines. Specifically, the output of a mode-locked laser is a train of ultra-short pulses corresponding to a phase-stable superposition of multiple longitudinal modes of the laser resonator. The frequencies of the longitudinal modes of a diffraction-limited laser are equidistantly separated by the laser's repetition rate (f_{rep}). To facilitate locking between the single frequency lasers and the frequency comb as well as to enable the generation of a frequency difference with high accuracy and precision, the oscillator's repetition rate, f_{rep}, as well as its carrier-envelope offset (CEO) frequency (f_{CEO}) must be fixed.

Then, phase-locked loops between each of the single frequency lasers and the frequency comb establish a fixed phase and frequency relation between the two single frequency lasers. Assuming that both single frequency lasers are locked at the same side of the teeth of the frequency comb, the resulting highly accurate, highly precise frequency difference is expressed as

$$\Delta\nu = \nu_2 - \nu_1 = N \cdot f_{rep} \tag{1}$$

The frequency difference is an exact integer (N) multiplier of the ultra-short pulse laser's repetition rate (f_{rep}). It exhibits sub-Hz frequency precision and accuracy. In time-domain, the coherent superposition of the two single frequency lasers corresponds to a phase-stable optical beat with beat frequency Δν.

Locking the lasers from different sides with respect to the teeth of the comb causes frequency differences with additional offsets of $\pm 2 \cdot f_{ref}$, where f_{ref} denotes the frequency of the RF reference clock as shown in Fig. 1(b). As explained in detail in the experimental section, f_{ref} is needed for the RF mixing in the phase-locked loops. The case of Eq. (1) is the goal since the subsequent DFG process cancels the phase-noise of the RF reference clock that is introduced via the phase-locked loop. Otherwise, it will double. Also, the case of Eq. (1) enables rapid and phase-sensitive detection of the optical beat or the multi-cycle terahertz waveform, as detailed in section 2.4.

2.2 Required system design for efficient terahertz generation

We generate picosecond pulses from the optical beat by using optical amplitude modulation. A frontend that produces optical beat pulses with picosecond durations is well suited for efficient generation of multi-cycle terahertz waves exhibiting a high-purity carrier frequency. For the example, this is required for the terahertz applications of compact electron acceleration [12]. The terahertz generation process provides guidelines for target parameters of the optical beat pulses. These shall be considered during the design of the laser frontend.

To produce high-field strength terahertz pulses, laser-based generation using high-energy lasers is necessary. Ytterbium-based lasers are attractive candidates since they can be efficiently pumped with high-brightness pump diodes and show low quantum defects leading to good thermo-optical properties, which in turn enable high average power and high-energy outputs. Ytterbium-based lasers have wavelengths around 1 µm.

For terahertz generation with 1-µm lasers, the nonlinear material of lithium niobate shows the highest figure-of-merit [13]. In lithium niobate, the large difference in refractive indices at the terahertz and laser frequencies results in a short coherence length. To enable coherent build-up of terahertz radiation over distances beyond the coherence length and thus optimize the conversion efficiency, quasi-phase matching using periodically poled lithium niobate (PPLN) is employed [14]. Absorption of lithium niobate is high in the terahertz spectral region [15]. Thus, the PPLN's length that can be applied for terahertz generation is limited by

Optics EXPRESS

the effective length due to absorption [16]. Cryogenic cooling decreases terahertz absorption. This enables longer PPLN lengths increasing conversion efficiency.

In PPLN, the difference in group indices at the terahertz and laser frequencies also result in walk-off. The walk-off length is directly proportional to the interaction time of the nonlinear conversion process [16]. Specifically, it is impacted by the duration of the optical driving pulse. To optimize the temporal overlap for the nonlinear interaction, the duration of the laser pulses must be appropriately set so that the corresponding walk-off length matches the crystal length (which is determined by the effective length due to absorption). For instance, the generation of terahertz at 300 GHz by a 1-µm laser in cryogenically cooled (80 K) 14-mm long PPLN requires laser-pulse durations > 150 ps [16,17]. Numerical calculations reveal optimum pulse durations of about 250 ps for terahertz frequencies of 300 GHz [17]. For reaching Joule-level pulse energies, however, longer pulse durations are desired to avoid damage in solid-state laser amplifiers. Although the conversion efficiencies reduce slightly with longer pulse duration (e.g. longer than 250 ps for ν_{THz} = 300 GHz), the total terahertz pulse energy produced can be higher. Assuming damage thresholds of the PPLN of order 1 J/cm^2, for >100 ps pulses, as has been previously reported [18], crystal apertures of area of about 1 cm^2 are needed. Fortunately, PPLN crystals of this size have recently been demonstrated [19]. This confirms that Joule-class lasers can be employed and are thus desired for terahertz generation at the cutting edge of energy and conversion efficiency.

In this contribution, we focus on the development of a laser frontend emitting optical beat pulses optimized for terahertz generation with shapeable envelope and picosecond durations. This frontend can serve as a seeder for subsequent high-energy booster amplifiers. To efficiently extract laser-pulse energy from a high-energy laser amplifier, it needs to be operated in saturation, which will cause a distortion of the laser pulse's shape. Pre-compensation of those pulse distortions is possible by shaping of the input pulse [20]. The present frontend enables such pulse shaping. Subsequent applications of multi-cycle terahertz pulses may have additional requirements on the shape of terahertz pulses.

2.3 Comparison of pulse-formats for efficient terahertz generation

In [17], different laser-pulse formats are compared in detail with regard to multi-cycle terahertz generation by numerical simulations. In practice, we expect that the present approach using optical beat pulses for generation of multi-cycle terahertz radiation has several advantages in comparison to generation using transform-limited or chirped-and-delayed broadband pulses:

Using ultra-short pulses in cryogenically-cooled PPLN, multi-cycle terahertz waveforms can be created [21], however, optical to multi-cycle terahertz conversion efficiency is limited by walk-off as explained in the preceding section [15]. The present frontend produces optical beat pulses with sub-0.5 ns durations. These long pulse durations increase the interaction length before walk-off occurs. And in this way, matching it better to the effective length due to absorption of the cryogenically cooled PPLNs. The increased interaction length for terahertz generation results in enhanced optical to terahertz conversion efficiency.

Using chirped-and-delayed pulses in cryogenically-cooled PPLN, one of the highest optical to terahertz conversion efficiencies have been demonstrated [22,23]. However, the precise control over the terahertz wave's frequency and its bandwidth is challenging. Particularly, in the presence of third- and higher-order dispersion during the chirping. Even in the case of a nearly perfect linear chirp that is generated using chirped fiber Bragg gratings (CFBG) or chirped Volume Bragg gratings (CVBG), refractive index variations will result in group-delay ripples [24], and in the case of bulk gratings spatial uniformity is a challenge. Also, during subsequent pulse amplification in laser amplifiers, the nonlinear effect of self-phase modulation will result in a nonlinear deformation of any linear chirp [25]. These effects and their combined action will have additional ramifications on the frequency-precision of the generated multi-cycle terahertz wave. For periodically-poled crystals with many periods, the

Optics EXPRESS

phase-matching bandwidth can restrict the portion of the spectrum that contributes to the terahertz generation process, limiting the conversion efficiency [26–28].

In the present approach, the single frequency lasers show line-widths (limited by the pulse envelope) that are smaller than the phase-matching bandwidth of the PPLN. There is no chirping of broadband pulses and the whole pulse (energy) contributes to the terahertz generation. The carrier to envelope phase of the terahertz pulse can be adjusted by pulse shaping in the optical domain. Moreover, the frequency difference (i.e., terahertz carrier frequency) can be set with Hz-level accuracy. Depending on the nonlinear medium used, frequency tunability in steps of f_{rep} is possible from a few GHz to multiple THz. The latter is also relevant for optimization of the conversion efficiency by tuning the line separation to the center frequency of the PPLN´s phase-matching. Besides precise frequency control, a system design based on a frequency comb also offers the additional advantage of rapid detection of the envelope of the synthesized waves by using synchronous optical sampling.

2.4 Rapid detection of the synthesized waveforms

In the optical domain, optical cross-correlation can be used for characterization of the envelope of the optical beat pulse. In the terahertz domain, electro-optical sampling is employed for detection of the multi-cycle terahertz pulse. For both methods, an ultra-short pulse serves as a reference. The frontend is based on a laser frequency comb. Thus, an ultra-short pulse reference is available for detection of the synthesized waveforms.

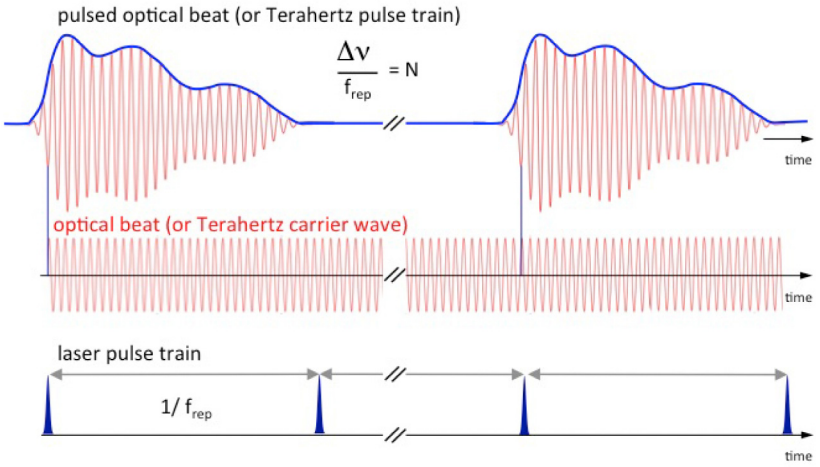

Fig. 2. Illustration of the optical beat (red line), generated optical beat pulse with an envelope created by amplitude modulation (blue line) and its relation to the ultra-short laser pulses of the optical frequency comb (bottom).

Equation (1) states that the ultra-short pulsed laser's repetition rate is an exact sub-harmonic of the synthesized beat frequency (or the terahertz pulse's carrier frequency). As illustrated in Fig. 2, this fact enables rapid and phase-sensitive detection. Note, the amplitude modulator is triggered by the repetition rate of the ultra-short pulse train f_{rep}. So, the modulator creates a synchronized train of optical beat pulses with a repetition rate that is a sub-harmonic of f_{rep}.

Furthermore, the pulse duration of the optical beat pulses is typically much shorter than $1/f_{rep}$. For instance, we are interested in production of optical beat pulses with durations < 0.5 ns, because it allows for efficient terahertz generation. During cross-correlation, a section of this optical beat pulse is sampled by the ultra-short pulse. Note, Fig. 2 can also be used to illustrate the electro-optical sampling of multi-cycle terahertz pulses by ultra-short pulses.

Optics EXPRESS

The situation is similar as the terahertz pulses are generated from the optical beat pulses by DFG.

The phase-locked loops and the integer relationship between the beat frequency (Δν) and the repetition rate of the ultra-short pulse train (f_{rep}) ensure that the timing of the optical beat signal's sinusoidal temporal-intensity profile is fixed relative the ultra-short pulse train. So, the optical beat's intensity value is the same for all pulses of the ultra-short pulse train. As mentioned before, the envelope of the optical beat pulse covers less than the pulse repetition interval ($1/f_{rep}$) and it occurs at a sub-harmonic of f_{rep}. The inherent synchronization implies that the relative timing between the envelope and the phase of the optical beating is the same for all optical beat pulses of the pulse train. So, we are guaranteed that the timing of the optical beat pulse's envelope is fixed relative to the optical beat signal's sinusoidal temporal-intensity profile. By the same argument, the carrier-envelope phase of the generated multi-cycle terahertz waveform is also fixed. The inherent synchronization of the optical beat to its envelope as well as to the ultra-short pulse train enables synchronous optical sampling of the optical beat pulse's intensity, or likewise of the resultant terahertz waveform, by the full ultra-short pulse train.

3. Experimental setup

3.1 Overview laser system

Figure 3 shows a schematic of the laser system. Figure 3(a) shows the phase-stable optical beat generation from a laser frequency comb. Figure 3(b) concerns the shaping of <0.5 ns long beat pulses from the continuous optical beat.

In the part of the system, shown in Fig. 3(a), we first lock the ultra-short pulse laser's repetition rate f_{rep} to an external 10 MHz reference oscillator. Second, a stable single-frequency laser is employed to fix the f_{CEO} of the ultra-short pulse train. It is an optical reference for our laser frequency-comb generation. Alternatively, one could also implement a 1f-2f interferometer to stabilize f_{CEO}. However, this approach requires super-continuum generation, which is not necessary for our application. The single frequency laser (Stable Laser Systems) used here, exhibits a very high stability (kHz per day) of its center frequency ν_1. Ideally, leading to a minimum CEO-phase fluctuation <2 μrad. A phase-locked loop ensures pinning of the comb to the stable laser's line by employing an acousto-optical frequency shifter in a feed-forward loop. The stabilized frequency comb serves then as a reference to lock the frequency of a second single-frequency laser. In this way, a phase-stable optical beat is produced.

3.2 Generation of a phase-stable optical beat

3.2.1 Repetition rate stabilization of the ultra-short pulse oscillator

The ultra-short pulse laser's repetition rate f_{rep} is stabilized to 70 MHz by locking it to an RF master clock with an RF mixer. The laser is based on a home-built NPE mode-locked Ytterbium-doped fiber laser. Details on this laser oscillator can be found in [29]. The free-running laser shows very slow (few-second time-scale) changes of the repetition rate. During the course of a day in our laboratory, we typically measure drifts of $\Delta f_{rep} < 100$ Hz in a free-running operation.

To lock the repetition rate, we detect the optical pulse train with a photo-diode (Thorlabs DET36A/M). As shown in Fig. 3(a), its output is split. One part monitors the performance of the locking (monitor repetition rate), e.g., by using an RF signal analyzer. The other part is sent to the RF mixer (Mini Circuits ZRPD-1 +) in which this signal is compared to a 70 MHz reference. This reference is derived from a combination of 10 MHz output from an oven-controlled crystal oscillator (OCXO) (InWave B-110), a 7x frequency multiplier (Mini Circuits RMK-7-81 + on PCB TB-393A) and a 70 MHz bandpass filter (Mini Circuits SXBP-70). The error signal of the RF mixer is amplified in two stages (each employing Mini

Optics EXPRESS

Circuits ZFL-1000-LN +). All RF components are powered by a low-noise power supply (Kniel CPM 0802/PFS). The error signal serves as an input to a proportional-integral (PI) servo controller (Newfocus LB1005) driving a single PZT stage (Piezosystems Jena PX38 with driver 12V40) that is built inside the ultra-short pulse oscillator. The PZT stage has a range of 38 µm, allowing path-length changes that are double this amount, since it is used in combination with a reflecting mirror. Thus, frequency changes of up to 1.2 kHz can be actively compensated.

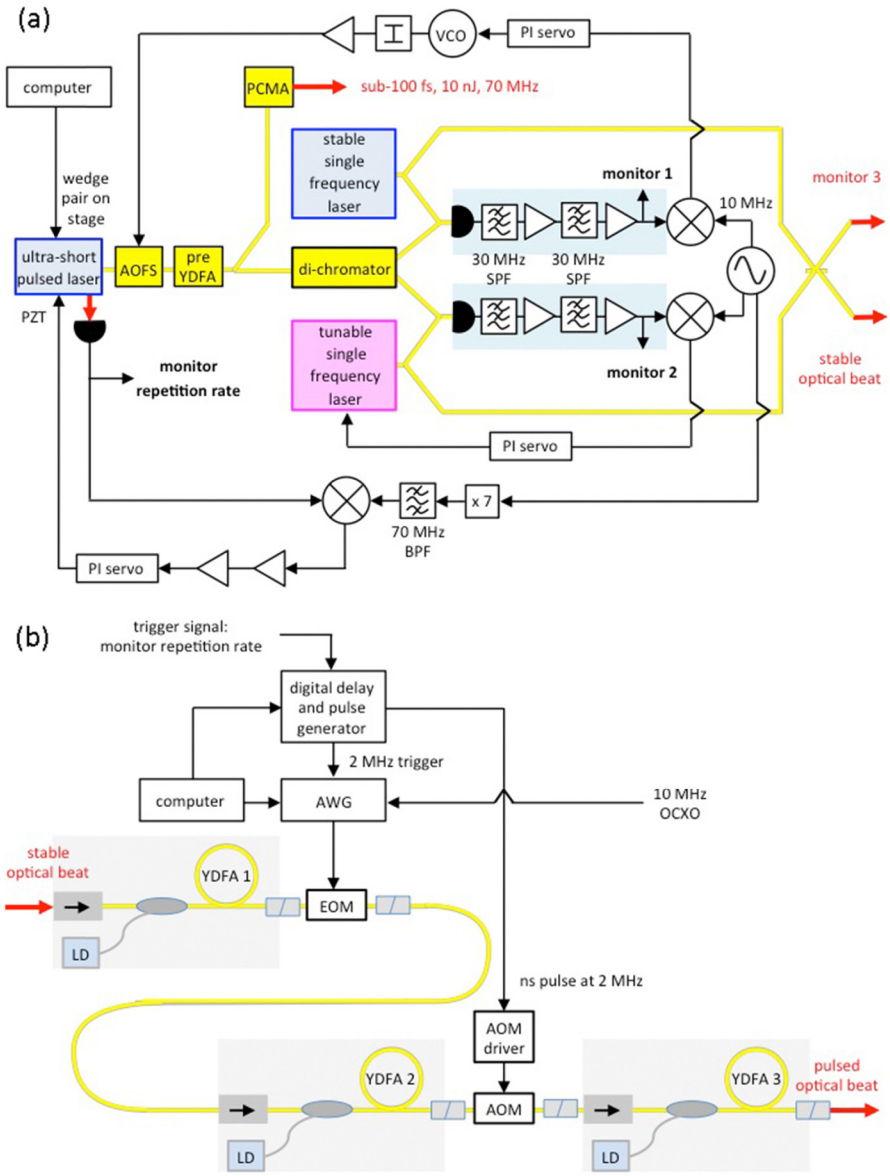

Fig. 3. Schematic of the experimental setup of the laser system containing pre-chirp managed amplifier (PCMA), voltage-controlled oscillator (VCO), acousto-optic frequency shifter (AOFS), radio frequency (RF) short-pass filters (SPF) and band-pass filters (BPF). Ytterbium-doped fiber amplifier (YDFA), arbitrary waveform generator (AWG), electro-optic modulator (EOM), acousto-optic modulator (AOM), 975nm single mode laser-diodes (LD).

Optics EXPRESS

3.2.2 Error signal generation for the phase-locked loops

As shown in Fig. 1(b), the single frequency lasers are phase-locked using a laser frequency comb. To generate error signals for the corresponding phase-locked loops, optical heterodyne detection between the frequency comb and each single frequency laser is employed. Then, the optical heterodyne signals are demodulated in RF mixers with the 10-MHz RF reference signal that is provided by the OCXO. The outputs from the RF mixers generate the error signals for feedback/ feedforward in the two phase-locked loops.

As shown in Fig. 1(b), only the beat between each single-frequency laser and the next single comb tooth is relevant for the mixing with the 10 MHz reference. Note, the comb teeth spacing is given by the locked repetition rate of f_{rep} = 70 MHz. So, the relevant frequency range of the optical heterodyne signal frequency is f_{rep} / 2. To improve the ratio of the optical heterodyne signal to the background in the range 0 - 35 MHz (as measured with a signal analyzer), an optical monochromator filters a section of the optical spectrum of the ultra-short pulse train in the vicinity of the single-frequency laser's center wavelength. Since two lines from the frequency comb are used for locking, a monochromator with two fiber-coupled, spectrally distinct outputs is employed. It is based on a 1600 l/mm grating (Lightsymth). In the following, we refer to this device as a "dichromator". Each output of the dichromator is combined with its corresponding single frequency laser using a PM-fiber coupler.

Behind the photo-diodes (Thorlabs DET36A/M) of both optical heterodyne detectors, the electrical signal is filtered and amplified (with a chain of Mini Circuits SLP-30, ZFL-1000-LN + , ZX75LP-30-S + , ZFL-1000-LN +), as shown in in Fig. 3(a). This signal is split before the RF mixer (Mini Circuits ZRPD-1 +): one part goes to the RF mixer. The other part serves as monitor allowing evaluation of the signal quality of the optical heterodyne detector as well as the locking performance by using a signal analyzer.

3.2.3 Frequency-comb generation by using an optical reference

One of the error signals is used to pin the CEO-frequency of the ultra-short pulse laser by using an optical reference in form of a stable single-frequency laser (Stable Laser Systems). Specifically, the stable laser consists of a single frequency laser that is locked to an ultra-stable reference cavity [30,31]. The output of this stable laser system is located around 1.03 µm and shows a linewidth of < 1 Hz and the center frequency' drift is as low as a few kHz per day.

Monitor 1, which is the auxiliary output from the optical heterodyne detector, permits characterization of the CEO-frequency with regard to the stable laser's frequency. The optical heterodyne detector results in a RF frequency (resulting from the beat between the stable laser and the tooth of the comb of the repetition-rate stabilized laser). This frequency is located in the range 0 – 35 MHz. For error signal generation by using the RF mixer and the 10-MHz RF-reference signal, an RF frequency of the optical heterodyne signal in the vicinity of 10 MHz is required.

To shift the mode-locked laser's CEO frequency without changing its repetition rate, we design and implement an isochronic wedge pair inside the laser's cavity [32]. Using the isochronic wedge pair, we can change the CEO-frequency with a minimal effect on the group-delay, and thus, the laser's repetition rate. Figure 4 shows the design of the employed isochronic wedge pair consisting of a glass wedge with an apex angle of 3° that is made of material 'N-LASF31A' as well as a glass wedge with an apex angle of 3.25° that is made of material 'N-SF6'. Both wedges of the pair have a maximum thickness of 2 mm. The wedges are oriented at Brewster angle for the first material to minimize Fresnel reflection losses. To change the CEO-frequency, the pair is moved in a direction that is perpendicular to the direction of the optical beam by using a computer-controlled translation stage (PI voice coil linear stage V-522.1AA with driver C-413.2GA). The adjustment of the CEO-frequency by the wedge pair sets the optical heterodyne detector's output signal in the vicinity of 10 MHz.

Optics EXPRESS

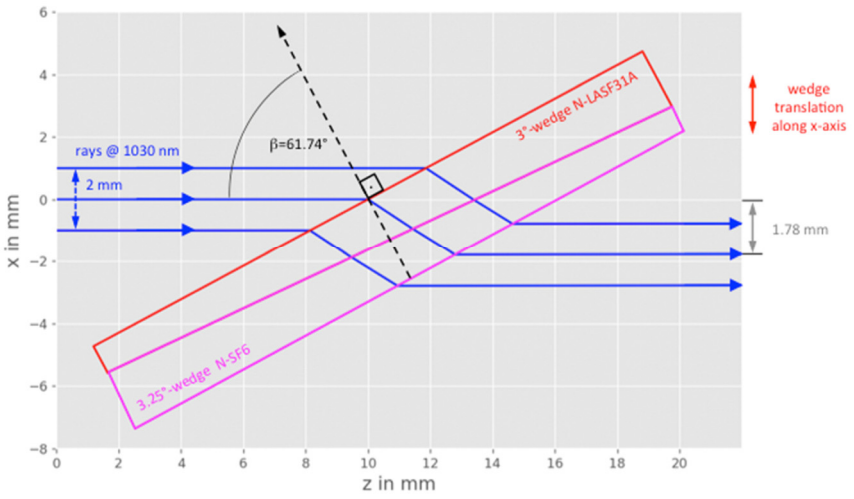

Fig. 4. Schematic of the iso-chronic wedge pair.

The resulting error signal enables closing of a feed-forward loop containing an acousto-optic frequency shifter (AOSF), which shifts the entire comb in frequency [33]. The error signal from the RF mixer is fed into a PI servo controller (Newfocus LB1005). Its output drives a voltage-controlled oscillator (VCO) (Mini Circuits ZX95-200-s +). The VCO´s output is attenuated (Fairview Microwave SA18E-11) and amplified (Mini Circuits ZHL-1-2W-S +) before it is connected to the fiber-pig-tailed AOFS (AA optoelectronics AA.MT110) enabling frequency shifts as large as +/– 10 MHz. In this way, the high frequency precision of the stable laser is transferred to the CEO-frequency leading to carrier-envelope-phase fluctuations much smaller than 1 mrad.

3.2.4 Locking a second (tunable) single frequency laser to the frequency comb

The resulting frequency comb serves as a reference for locking a second single frequency laser in terms of frequency and phase using optical heterodyne detection. The second laser is an external cavity laser diode (Toptica DL pro), which is (manually) tunable in the wavelength range from approximately 1000 nm to 1080 nm. In the following, the stable single-frequency laser and the second (tunable) single-frequency lasers are denoted, respectively, SFLl and SFL2. We set SFL2's wavelength approximately 1 nm apart from the stable laser's center wavelength. Fine-tuning of SFL2 is possible by a PZT and/or pump current modulation. For the locking of SFL2, we exclusively use the pump current modulation as it allows tuning of several tens of MHz with high bandwidth (approx. MHz). The PI servo controller's output is directly connected to the pump-modulation port at the SFL2's laser head.

Due to the broad wavelength-tunability of SFL2, the locking frequencies chosen from the frequency comb can be varied. As illustrated in Fig. 1(b), the locking frequencies are spaced by the repetition rate (here 70 MHz). Note, for wider tuning of SFL2 the bandpass transmission window of the dichromator must be adjusted accordingly.

Use of a frequency comb thus enables achievement of phase-stability between two single-frequency lasers separated in frequency by several hundreds of GHz or even multiple THz. In both phase-locked loops, the RF mixer introduces the phase-noise of the OXCO's RF reference signal (at 10 MHz). To produce a low-phase noise difference frequency signal in the terahertz region, it is important to cancel this noise by the DFG process. This is achieved by locking SFL1 and SFL2 from the same side to the frequency comb, as illustrated in Fig. 1(b). In this way, the resulting terahertz signal is free of the RF reference's phase-noise.

Optics EXPRESS

Moreover, its frequency is an integer multiplier of the ultra-short pulse laser's repetition rate f_{rep}, which is needed for synchronous sampling, as explained in section 2.4.

3.3 Generation of picosecond pulses from the stable optical beat

As shown in Fig. 3(b), the temporal envelope of the beat pulses is generated from the continuous optical beat by amplitude modulation. For this, we employ a combination of an electro-optic modulator (EOM) and an acousto-optic modulator (AOM). The fiber-pigtailed modulators are sandwiched between Ytterbium-doped fiber amplifiers (YDFA) to enable amplification of the desired frequencies while minimizing the growth of spontaneous emission. All passive fibers of the setup are single mode and polarization maintaining (PM980).

The YDFAs are all core-pumped, polarization maintaining (PM), highly doped, single-mode fibers (coreactive Yb501-PM) with length of approximately 50 cm. At the input, optical isolators are inserted to protect the optical modulators or preceding amplification stages from unwanted back-propagating signal. Note, Brillouin scattering is not an issue since the effective bandwidth of the two-color signal is much larger (for instance 300 GHz line-to-line separation) than the bandwidth of the Brillouin gain spectrum, which is approximately 50 MHz for silica fibers [34].

The EOM (iXblue modbox) offers computer-programmable pulse shaping by using an arbitrary waveform generator (AWG). It is PM-fiber pigtailed and exhibits a high extinction ratio > 55 dB (at 1030 nm). Its AWG offers a maximum frequency of 2 MHz, 12 bits resolution, maximum D/A rate of 4 GS/s, maximum memory size of 4 MS (1ms), the temporal jitter is 30 ps and the rise time is 60 ps. Note, the EOM is a bottleneck for the power amplification: first, the shaping of a rectangular pulses with durations below 0.5 ns at a 2 MHz repetition rate (i.e. 500 ns pulse-to-pulse separation) leads to a duty cycle of 1/1000. Second, the insertion loss is approximately 12 dB. Additional losses up to 10 dB may arise due to the biasing of the modulator. Third, the maximum optical (average) input power of the EOM is 200 mW. To increase the power at the EOM's output (i.e. the input power for the following amplifier), a longer auxiliary pulse with duration of several ns can be created approximately 20 ns after the pulse of interest.

To enhance the contrast between the generated pulses of interest and to eliminate the auxiliary pulses, a fiber-pigtailed AOM (AA optoelectronic MT200) is employed. It is a 200 MHz TeO_2 AOM with a rise time of around 10 ns. Its analog driver receives a gate-pulse at 2 MHz from the digital delay and pulse generator (Stanford Research Systems DG645). Note, another output port of the digital delay and pulse generator is connected to the trigger input of the EOM´s AWG. In this way, the two modulators are synchronized. The delay that is sent to the AOM's driver is adjusted in such a way that only the pulses of interest are gated.

3.4 Characterization of the picosecond optical beat pulses by digital delaying

The pulsed optical beat is characterized using the method of optical cross-correlation. To sample the relatively long pulses, sub-100fs pulses are used. These reference pulses are obtained from the compressed output of the pre-chirp managed amplifier (PCMA), as shown in Fig. 3(a). Details of the PCMA's design can be found in [29,35]. The second harmonic for the optical cross-correlation is generated in a 1 mm long BBO crystal (cut for type I phase-matching) in a non-collinear geometry. Note, the sub-100 fs reference pulses have a pulse repetition rate of 70 MHz and the pulses of the optical beat have a repetition rate of 2 MHz. Therefore, optical beat pulses as long as about 14 ns (i.e. 1/ 70MHz) can be characterized, see also Fig. 2.

As shown in Fig. 3(b), both the EOM's AWG and AOM's driver signals are generated by the digital delay and pulse generator, and additionally, are synchronized to the ultra-short pulse train. Specifically, the ultra-short pulse's repetition rate (stabilized to 70 MHz) serves as a trigger to the digital delay generator.

Optics EXPRESS

This scheme enables rapid characterization of the envelope of the optical beat pulses by electronic temporal delaying. The AWG generates the electronic waveform that is applied to the EOM, which in turn determines the envelope of the optical beat pulse. A delay of the AWG's trigger signal will temporally shift the position of the envelope. Note, the AWG is also referenced to the OCXO´s 10 MHz external clock. Using computer control of the digital delay generator, a common delay is applied to both the AWG's trigger and the AOM's driver signal. The minimum delay step can be as low as 1 picosecond. In this way, the envelope of the optical beat pulse can be temporally shifted with respect to the ultra-short pulse train at the cross-correlator.

This electronic scanning method has the following advantages over mechanical delay lines: first, the temporally delayed beam does not experience transverse beam shifts even for delays on ns-time scales. This ensures constant overlap of the two beams at the nonlinear crystal, resulting in clean signals. Second, the electronic temporal scanning is much faster (typically less than 1 s acquisition time for the complete cross-correlation trace covering a time window as large as several ns).

4. Experimental results

4.1 Frequency-comb generation

4.1.1 Repetition-rate locking

As described in section 3.2.1, the error signal for the repetition rate loop is generated by demodulation of the photo-diode signal (monitor repetition rate) with a RF mixer using a RF reference signal. This reference is a 250 mV peak-to-peak 70 MHz signal, which is available after the 70-MHz RF-bandpass filter and x7 frequency multiplier, as shown in Fig. 3(a). For frequencies below 10 Hz, the phase-noise spectrum (not shown) of the x7 frequency multiplied 10-MHz OCXO has lower values as compared to that of the photo-detector signal of ultra-short oscillator pulse train (monitor repetition rate of the free-running oscillator). Thus, the locking point is set to about 10 Hz. Note, the OCXO's phase-noise at 10 MHz is specified < −118 dBc/Hz at 10 Hz and < −149 dBc/Hz at 100 Hz. Its Allan deviation is measured $< 2 \cdot 10^{-11}$ for $\tau > 2$ s. For the closed repetition-rate feedback loop, Fig. 5 shows a typical RF spectrum of the monitor repetition rate at the signal analyzer. It is recorded in a 1-kHz frequency span and the center frequency is exactly 70 MHz. Due to the long range of the PZT stage, as described in section 3.2.1, and the very good temperature stability of the lab (around 1°C), excellent long-term (i.e. months) locking performance is available.

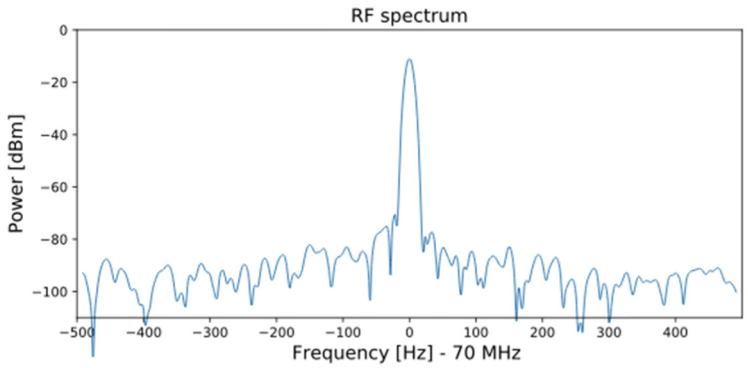

Fig. 5. RF spectrum at the signal analyzer showing the stabilized repetition rate.

Optics EXPRESS

4.1.2 Characterization of the isochronic wedge pair

As mentioned in section 3.2.3, the isochronic wedge pair shifts the optical heterodyne signal to the vicinity of the target RF frequency of 10 MHz, which corresponds to the OCXO's reference output.

To characterize the wedge pair, we first measure the residual effect of the translation of the wedge pair on the repetition rate. For this, the repetition-rate locking of the ultra-short pulse oscillator is turned off. Note, the repetition-rate fluctuations of the free-running oscillator are only a few Hz on a minute timescale, as demonstrated later in Fig. 9(a). The repetition rate is measured using a signal analyzer (Agilent CXA N9000A) that is connected to the monitor repetition rate, which is shown in Fig. 3(a). The peak positions of the RF spectra (similar to the one that is displayed in Fig. 5) are read out with a computer for different translation stage positions. The frequency precision of this measurement is as good as 1 Hz. The wedge pair's stage's position is read out with a built-in encoder. Figure 6 shows the change of repetition rate as a function of wedge-pair translation, which is perpendicular to the optical beam path. As can be seen from Fig. 6, the residual change of repetition rate is as small as 13 Hz for a 1 mm translation. When the repetition-rate locking loop is closed the PZT actuator simply compensates such residual variations. They are 100x lower than the PZT's range. In this way, the CEO frequency can be smoothly adjusted without breaking the repetition rate lock.

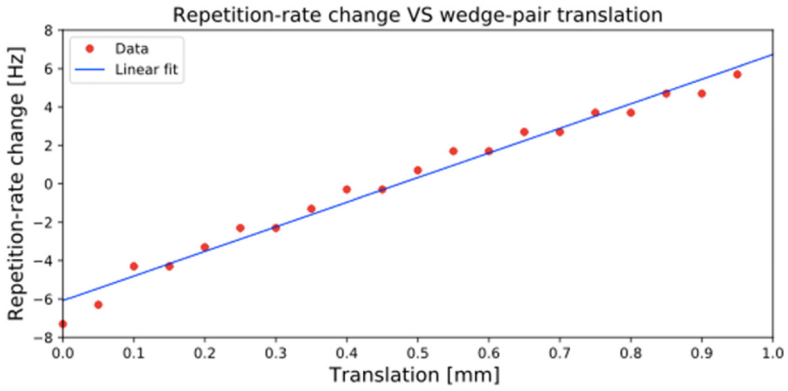

Fig. 6. Residual effect of the isochronic wedge pair's translation on the repetition rate of the free-running ultra-short pulse oscillator.

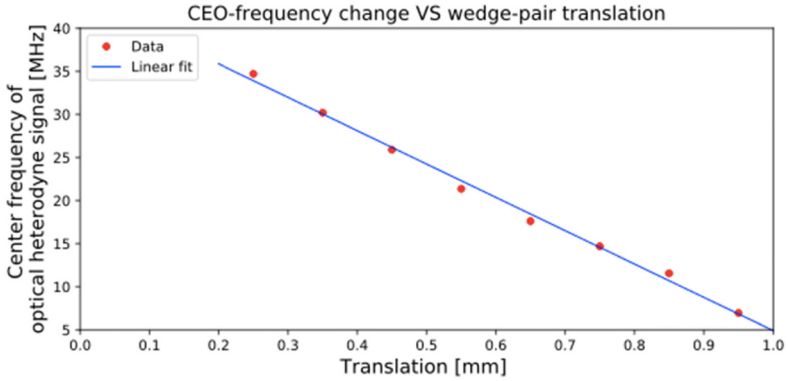

Fig. 7. Effect of the isochronic wedge pair's translation on the CEO frequency of the repetition rate stabilized ultra-short pulse laser oscillator.

Optics EXPRESS

Figure 7 shows the effect of the isochronic wedge pair's translation on the frequency of the optical heterodyne detection signal (monitor 1). To reveal the wedge pair's impact on the CEO-frequency, the repetition rate must be stabilized. For different translation-stage positions, the change of optical heterodyne detection signal is mainly due to the imposed change of CEO-frequency by the wedge-pair translation since the variation of the output frequency of the stable laser is very small (typical a few kHz during the course of a day). The peak of the RF spectrum of the optical heterodyne detection signal as well as the stage position are simultaneously read-out with a computer. As shown in Fig. 7, the change of CEO frequency with translation is 39 MHz/mm.

Direct CEO-frequency locking with the wedge pair was not possible since the bandwidth due to the stage movement is insufficient to compensate for rapid CEO-frequency fluctuations. However, the wedge pair brings the CEO-frequency to a position from which locking with the AOFS can be initiated.

4.1.3 Characterization of the AOFS

The frequency shifting of the AOFS is characterized as follows. First, the VCO's output drives the AOFS and its RF frequency is measured with a RF signal analyzer as a function of input voltage. Specifically, this voltage is varied by the PI controller's offset control. Second, the optical transmittance through the AOFS is measures as a function of PI controller's output voltage. Figure 8 shows the resulting optical transmission as a function of applied RF frequency. The frequency of the diffracted first-order optical beam in the AOFS is frequency-shifted by this acoustic carrier frequency [33]. As displayed in Fig. 8, the AOFS allows shifting of up to +/– 10 MHz (1 dB loss level on top of the 3 dB insertion loss) around a frequency offset of 107 MHz. Power fluctuations because of the frequency shifting are compensated by operating the subsequent Ytterbium-doped fiber amplifier in saturation.

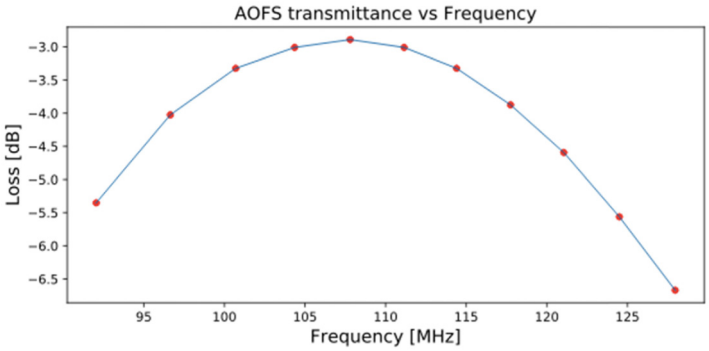

Fig. 8. Transmittance through the AOFS as a function of frequency (the red dots are the measurement data).

4.1.4 Frequency-comb generation

The ultra-short pulse oscillator is characterized for the different states of the two locking loops by monitoring the optical heterodyne detection signal with the stable laser (monitor 1). Figure 9 shows the frequency of the peak of the optical heterodyne detector signal during a measurement of 5 min. The frequency of the peak is read-out from the signal analyzer with a computer. The frequency range of this measurement is located in the range from 0 to f_{rep} /2.

Figure 9(a) shows the case of a free running ultra-short pulse oscillator. The fluctuations are mainly due to fluctuations in repetition rate. Any frequency change of the repetition rate (around 70 MHz) is multiplied by a factor of approximately $4 \cdot 10^6$ when observed in the optical domain around 1030 nm. Using the exact multiplier, the peak-to-peak fluctuations of the repetition rate of the free running oscillator are determined to be as low as 4 Hz during 5 min.

Optics EXPRESS

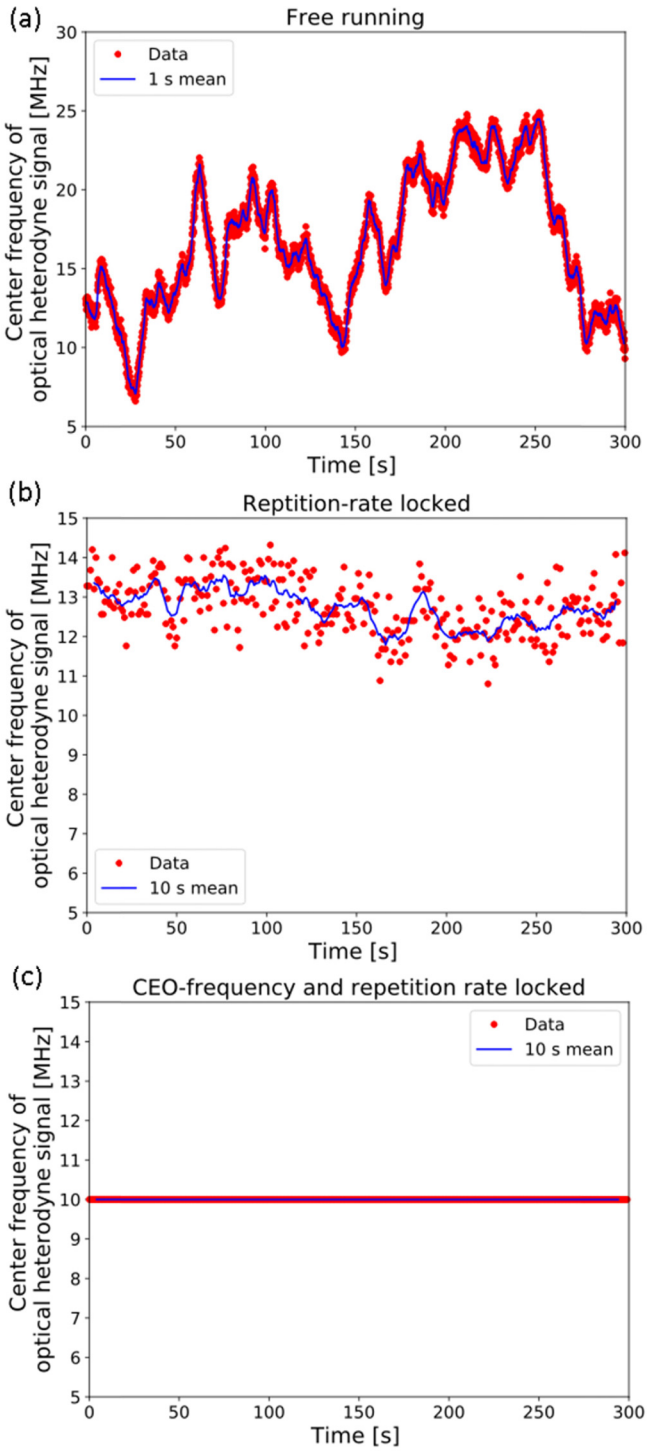

Fig. 9. Time-dependent behavior of the center frequency of the optical heterodyne detection signal for the case of (a) free running ultra-short pulse oscillator, (b) repetition-rate locked ultra-short pulse oscillator, and (c) additional fixing of CEO-frequency to the stable laser in feed-forward scheme.

Optics EXPRESS

Figure 9(b) shows the frequency of the peak of the optical heterodyne detector signal when the repetition rate is locked. Compared to Fig. 9(a), the y-axis is rescaled. The fluctuations due to un-stabilized CEO-frequency have an RMS of 0.7 MHz. The resolution bandwidth of the signal analyzer is 91 kHz (for a RF span of 10 MHz).

Figure 9(c) shows the impact of the CEO-frequency locking on the optical heterodyne detection signal. The feed-forward loop with the AOFS uses a PI corner frequency of 30 kHz. The data in Fig. 9(c) shows residual fluctuations of 112 Hz (rms). However, this measurement is limited by the resolution bandwidth of the signal analyzer, which is 4.9 kHz (for a RF span of 500 kHz). Measurements with sub-Hz precision should be possible with a frequency counter.

4.1.5 Locking a second (tunable) single frequency laser to the frequency comb

Figure 10 illustrates an initial period of locking of both the CEO-frequency and the second single frequency laser (SFL2). The peak frequencies of the two corresponding optical heterodyne detection signals, which are displayed via RF spectra on signal analyzers, are simultaneously read out with a computer. As can be seen, both locking loops stabilize the optical beat frequencies to 10 MHz, which corresponds to the RF mixer's reference input, i.e. the OCXO's output. First, the AOFS stabilizes the optical heterodyne detection signal with SFL1 (red curve), and thus, fixes the CEO-frequency. A frequency comb is generated. Then, SFL1 is locked to the comb (blue curve).

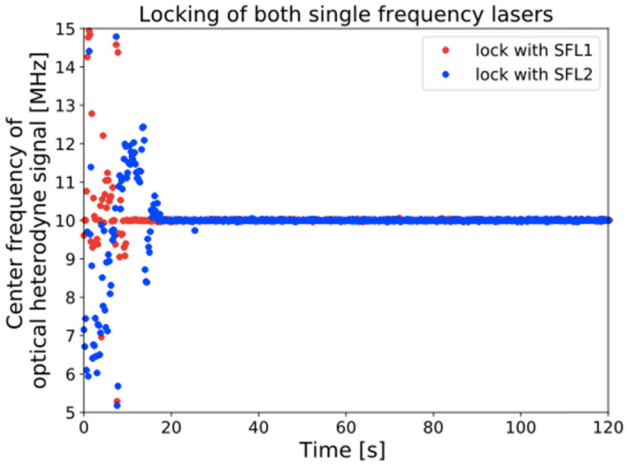

Fig. 10. Time-dependent behavior of the center frequencies of the two optical heterodyne detection signals with SFL1 and SFL2.

4.2 Computer-programmable pulse generation from the continuous optical beat

As detailed in section 3.3, beat pulses with hundreds of picosecond durations are generated from the continuous optical beat by optical amplitude modulation. As mentioned before, the EOM's AWG exhibits a D/A rate of 4GS/s. Thus, the minimum temporal increment is 250 ps. Figure 11(a) shows the values that are loaded into the EOM's AWG. The expected rise and fall times are not shown in Fig. 11. The manufacturer specifies a rise/ fall time of 60 ps.

Figure 11(b) shows the pulse measurement with a 22 GHz photodiode (Semiconductor Discovery Lab Buddy DSC-30-S-HLPD) and a wide bandwidth (> 100 GHz) oscilloscope (Agilent DCA-X 86100D). To avoid saturation of the photo diode, the measurement is performed directly after the AOM. The (mean) measured pulse duration is 363 ps (FWHM). The average output power after the third YDFA, as shown in Fig. 3(b), is 50 mW, the pulse-repetition rate is 2 MHz.

Optics EXPRESS

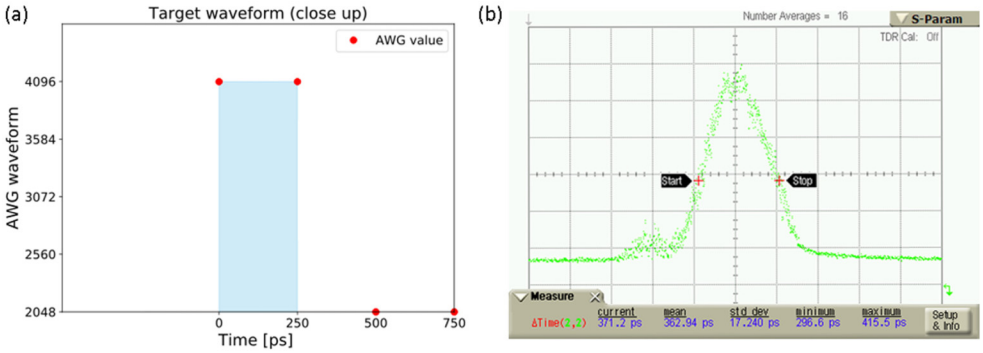

Fig. 11. (a) Target waveform loaded into AWG, (b) measurement of the resulting pulse by using high bandwidth photo-detector and oscilloscope.

4.3 Cross-correlation of the optical beat pulses

As described in section 3.4, the synthesized waveforms can be also characterized using optical cross-correlation. The ultra-short pulse output from the PCMA amplifier samples the sub-ns optical beat pulses. Figure 12 shows the autocorrelation of the ultrashort pulse (measured with APE autocorrelator). The ultra-short pulse train at the output of the PCMA amplifier shows an average power as high as 830 mW and its repetition rate is 70 MHz. The optical beat pulse's repetition rate is 2 MHz.

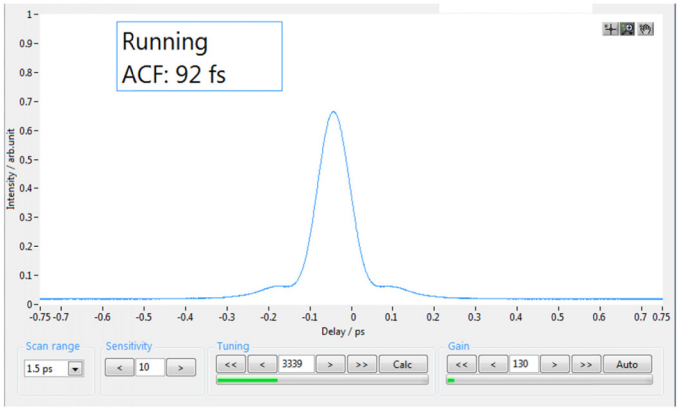

Fig. 12. Auto-correlation of the ultra-short pulse that samples the optical beat pulse via optical cross-correlation.

To perform the cross-correlation, the optical beat pulse's envelope is digitally delayed with respect to the ultra-short pulse train by using a digital delay and pulse generator. Figure 13 shows the result of the optical cross-correlation. During the measurement, the step size of the digital delay is 10 ps. In principle, it can be as low as 1 ps. The acquisition time of each point is approximately 1 ms in this proof-of-principle experiment. Thus, the acquisition of the whole trace is typically completed within seconds depending on chosen delay span and step-size. The measured pulse duration (FWHM) is 420 ps.

Optics EXPRESS

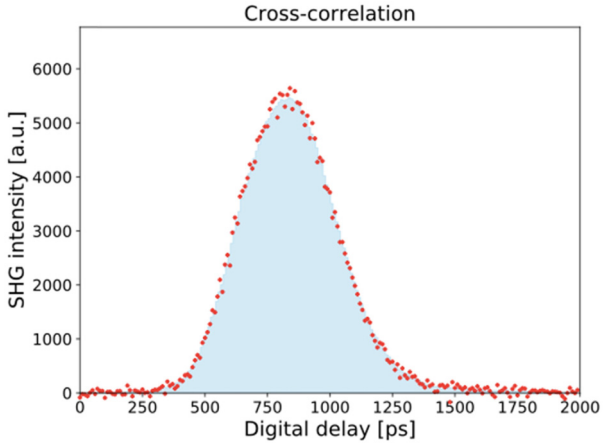

Fig. 13. Optical cross-correlation of the optical beat pulse.

4.4 Auto-correlation of the optical beat pulses

The optical cross-correlation using digital delaying reveals the envelope of the optical beat pulse. However, it cannot determine the beat modulation. This is because both the beat frequency and the repetition rate of the optical beat pulse are derived from the ultra-short pulse's repetition rate, as given by Eq. (1). The optical modulators modulate the envelope of the optical beat. Thus, this leaves the relative timing between beat wave's modulation and the ultra-short pulse unchanged, as illustrated in Fig. 2.

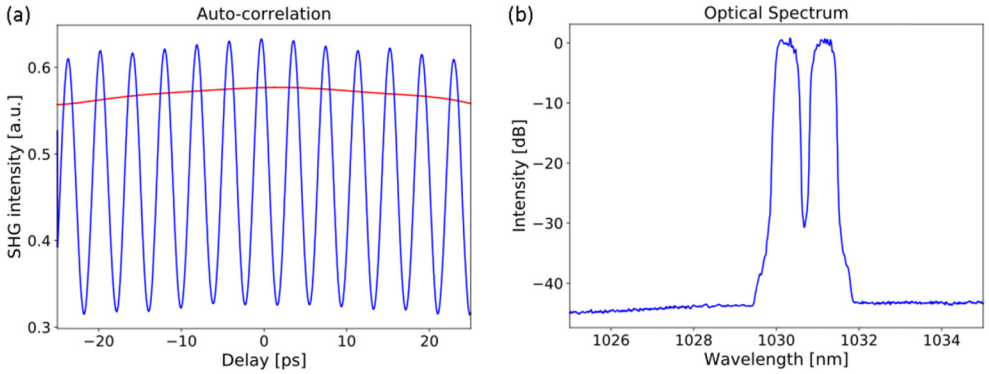

Fig. 14. (a) Optical auto-correlation of the central section of the optical beat pulse, and (b) corresponding optical spectrum of the two lines.

To determine the beat wave's modulation, we perform an autocorrelation of the optical beat pulse, as shown via the blue curve in Fig. 14(a). To verify that the modulations in the autocorrelation are indeed due to the optical beat, we turn off one of the single-frequency lasers. In this case, the modulation is not present in the autocorrelation, as shown via the red curve in Fig. 14(a). Due to the limited delay range of the autocorrelator for this measurement of 420 ps long pulses, only a section of the auto-correlation can be recorded. The temporal spacing between consecutive maxima in the autocorrelation is determined as 3.93 ps. This corresponds to a frequency difference $\Delta\nu$ of 0.255 THz (or 0.9 nm) between the peaks of the single-frequency lasers at 1030 nm. This finding agrees with the optical spectrum of the two laser lines, as shown in Fig. 14(b). Note, the widths of the optical lines appear broader due to the resolution limit of the optical spectrum analyzer (Ando AQ6317B).

Optics EXPRESS

5. Conclusion

We have demonstrated a laser system producing optical beat pulses with hundreds of picosecond duration. The pulse parameters are designed towards multi-cycle terahertz wave generation using DFG in PPLN crystals. For the first time, to the best of our knowledge, we have demonstrated and characterized a computer-programmable envelope of an optical beat pulse at 1.03 µm with a duration as short as about 400 ps and a pulse-repetition rate as high as 2 MHz. Phase-locking of two single frequency lasers with their center frequencies hundreds of GHz apart is accomplished by using a frequency comb at 1030 nm. In our demonstration, the beat frequency is around 255 GHz. We measure a residual frequency variation of the laser-line locking at Hz-level. The measurement was limited by the RF spectrum analyzer' resolution.

We have built the frequency comb by using a feed-forward loop with an acousto-optical frequency shifter and an optical reference in form of a stable single frequency laser exhibiting frequency drifts of as low as kHz during the course of a day. For coarse adjustment of the CEO frequency, we employ for the first time – to the best of our knowledge – an isochronic wedge pair inside an ultra-short pulse Ytterbium-doped fiber laser. We measure a CEO-frequency change of 39 MHz and a residual repetition-rate change as low as 13 Hz for 1 mm (perpendicular to beam) wedge translation. This type of coarse adjustment of the CEO frequency is necessary to close the feed-forward loop with the AOFS without losing the repetition rate lock.

We have demonstrated swift detection of the envelope of the optical beat pulse using optical cross-correlation and digital delaying. It builds on an advantageous feature of the frequency-comb-based laser system, namely, that the ultra-short pulse laser's repetition rate is an exact sub-harmonic of the optical beat frequency. Using this inherent synchronization, we show optical beat pulse characterization by full electronic digital delaying of the optical beat pulse's envelope. It avoids mechanically moving parts, which would lead to beam-displacements (and thus signal fluctuations) and long acquisition times. In this way, envelopes with durations as long as the inverse of the repetition rate of the ultrafast pulse train can be synchronously sampled in as short as a few seconds by the ultra-short pulses. To characterize the envelopes of multi-cycle terahertz waveforms, a combination of electro-optical sampling and the electronic delaying method should be utilized. Thus, a frequency-comb-based laser source enables not only the generation of arbitrarily amplitude-shaped multi-cycle terahertz pulses (with high-precision carrier frequency) but can also be used for phase-sensitive, synchronous optical sampling of those.

Future efforts will primarily focus on the generation of a laser output comprising multiple lines. As explained in [17,36], a coherent superposition of multiple lines increases the conversion efficiency for multi-cycle terahertz generation. The multiple lines can be generated from the present system by coupling the front-end's output into a nonlinear fiber. The intensity-dependence of the refractive index of the waveguide will transfer the intensity modulation of the beat into an 'ultrafast' temporal phase modulation creating spectral side-bands [27,37]. This multi-line output exhibits a line-to-line spacing of the beat frequency. In this way, terahertz efficiency scaling can be demonstrated.

Future work will be concerned with increasing the energy of the optical beat pulse. Specifically, the laser system's pulse parameters constitute a suitable input for regenerative amplification to multi-mJ energies. Note, that the ultra-short pulse laser's repetition rate of 70 MHz is compatible with rise times of Pockels cells. For efficient extraction, these subsequent high-energy amplifiers are operated in saturation. However, saturation will cause distortion of the laser system's output pulses. The pulse-shaping capability of the EOM's AWG allows pre-compensation of these pulse distortions [20].

Emphasis will also be placed on a highly precise measurement of the frequency difference. For this a combination of optical and RF measurements is required. Using the current RF characterization, it is cumbersome to determine if the two single frequency lasers

Optics EXPRESS

are locked at the same side with respect to the teeth of the frequency comb (see also Fig. 1(b)). However, the benefit of the RF characterization of the optical heterodyne signal is its high (Hz-level) precision. Using an optical wavemeter, the wavelengths of the locked lasers can be measured as accurate as a few MHz. Thus, it can be determined if the frequency difference of the locked single frequency lasers is either an exact integer multiplier of the repetition rate or if it corresponds to undesired cases with additional frequency offsets. We expect that by employing additional RF characterization using high precision frequency counters (e.g. from Pendulum Instruments), measurements with Hz precision can be achieved locally. In this way, deterministic generation of THz-scale frequency differences with Hz precision and accuracy is possible. This will enable multi-cycle terahertz wave generation and characterization of hitherto unprecedented precision and accuracy. In turn, this will open up broad new avenues for the application of terahertz photonics.

Funding

Helmholtz Association through DESY and the Center for Free-Electron Laser Science; European Research Council under the European Union's Seventh Framework Programme (FP/2007-2013) / ERC Grant Agreement n. 609920; Cluster of Excellence: The Hamburg Centre for Ultrafast Imaging-Structure, Dynamics and Control of Matter at the Atomic Scale of the Deutsche Forschungsgemeinschaft.

References

1. J. F. Federici, B. Schulkin, F. Huang, D. Gary, R. Barat, F. Oliveira, and D. Zimdars, "THz imaging and sensing for security applications – explosives, weapons and drugs," Semicond. Sci. Technol. **20**(7), S266–S280 (2005).
2. E. Pickwell and V. P. Wallace, "Biomedical applications of terahertz technolopgy," J. Phys. D Appl. Phys. **39**(17), R301–R310 (2006).
3. T. Nagatsuma, S. Horiguchi, Y. Minamikata, Y. Yoshimizu, S. Hisatake, S. Kuwano, N. Yoshimoto, J. Terada, and H. Takahashi, "Terahertz wireless communications based on photonics technologies," Opt. Express **21**(20), 23736–23747 (2013).
4. L. J. Wong, A. Fallahi, and F. X. Kärtner, "Compact electron acceleration and bunch compression in THz waveguides," Opt. Express **21**(8), 9792–9806 (2013).
5. E. A. Nanni, W. R. Huang, K.-H. Hong, K. Ravi, A. Fallahi, G. Moriena, R. J. Dwayne Miller, and F. X. Kärtner, "Terahertz-driven linear electron acceleration," Nat. Commun. **6**(1), 8486 (2015).
6. W. Ronny Huang, A. Fallahi, X. Wu, H. Cankaya, A.-L. Calendron, K. Ravi, D. Zhang, E. A. Nanni, K.-H. Hong, and F. X. Kärtner, "Terahertz-driven, all-optical electron gun," Optica **3**(11), 1209–1212 (2016).
7. J. Capmany and D. Novak, "Microwave photonics combines two worlds," Nat. Photonics **1**(6), 319–330 (2007).
8. V. Torres-Company and A. M. Weiner, "Optical frequency comb technology for ultra-broadband radio-frequency photonics," Laser Photonics Rev. **8**(3), 368–393 (2014).
9. A. J. Seeds, M. J. Fice, K. Balakier, M. Natrella, O. Mitrofanov, M. Lamponi, M. Chtioui, F. van Dijk, M. Pepper, G. Aeppli, A. G. Davies, P. Dean, E. Linfield, and C. C. Renaud, "Coherent terahertz photonics," Opt. Express **21**(19), 22988–23000 (2013).
10. U. Demirbas, R. Uecker, J. G. Fujimoto, and A. Leitenstorfer, "Multicolor lasers using birefringent filters: experimental demonstration with Cr:Nd:GSGG and Cr:LiSAF," Opt. Express **25**(3), 2594–2607 (2017).
11. T. Yerebakan, U. Demırbas, S. Eggert, R. Bertram, P. Reiche, and A. Leitenstorfer, "Red-diode-pumped Cr:Nd:GSGG laser: two-color mode-locked operation," J. Opt. Soc. Am. B **34**(5), 1023–1032 (2017).
12. F. X. Kärtner, F. Ahr, A.-L. Calendron, H. Çankaya, S. Carbajo, G. Chang, G. Cirmi, K. Dörner, U. Dorda, A. Fallahi, A. Hartin, M. Hemmer, R. Hobbs, Y. Hua, W. R. Huang, R. Letrun, N. Matlis, V. Mazalova, O. D. Mücke, E. Nanni, W. Putnam, K. Ravi, F. Reichert, I. Sarrou, X. Wu, A. Yahaghi, H. Ye, L. Zapata, D. Zhang, C. Zhou, R. J. D. Miller, K. K. Berggren, H. Graafsma, A. Meents, R. W. Assmann, H. N. Chapman, and P. Fromme, "AXSIS: Exploring the frontiers in attosecond X-ray science, imaging and spectroscopy," Nucl. Instrum. Methods Phys. Res. A **829**, 24–29 (2016).
13. K. L. Vodopyanov, "Optical THz-wave generation with periodically-inverted GaAs," Laser Photonics Rev. **2**(1-2), 11–25 (2008).
14. R. W. Boyd, *Nonlinear Optics* (Academic Press, 2008), Chap. 2.
15. L. Pálfalvi, J. Hebling, J. Kuhl, Á. Péter, and K. Polgár, "Temperature dependence of the absorption and refraction of Mg-doped congruent and stoichiometric $LiNbO_3$ in the THz range," J. Appl. Phys. **97**(12), 123505 (2005).
16. K. L. Vodopyanov, "Optical generation of narrow-band terahertz packets in periodically inverted electro-optic crystals: conversion efficiency and optimal laser pulse format," Opt. Express **14**(6), 2263–2276 (2006).
17. K. Ravi, D. N. Schimpf, and F. X. Kärtner, "Pulse sequences for efficient multi-cycle terahertz generation in periodically poled lithium niobate," Opt. Express **24**(22), 25582–25607 (2016).

Optics EXPRESS

18. W. Koechner, *Solid-State Laser Engineering* (Springer, 1996).
19. H. Ishizuki and T. Taira, "Half-joule output optical-parametric oscillation by using 10-mm-thick periodically poled Mg-doped congruent LiNbO3," Opt. Express **20**(18), 20002–20010 (2012).
20. D. N. Schimpf, C. Ruchert, D. Nodop, J. Limpert, A. Tünnermann, and F. Salin, "Compensation of pulse-distortion in saturated laser amplifiers," Opt. Express **16**(22), 17637–17646 (2008).
21. S. Carbajo, J. Schulte, X. Wu, K. Ravi, D. N. Schimpf, and F. X. Kärtner, "Efficient narrowband terahertz generation in cryogenically cooled periodically poled lithium niobate," Opt. Lett. **40**(24), 5762–5765 (2015).
22. F. Ahr, S. W. Jolly, N. H. Matlis, S. Carbajo, T. Kroh, K. Ravi, D. N. Schimpf, J. Schulte, H. Ishizuki, T. Taira, A. R. Maier, and F. X. Kärtner, "Narrowband terahertz generation with chirped-and-delayed laser pulses in periodically poled lithium niobate," Opt. Lett. **42**(11), 2118–2121 (2017).
23. G. Tóth, J. A. Fülöp, and J. Hebling, "Periodically intensity-modulated pulses by optical parametric amplification for multicycle tunable terahertz pulse generation," Opt. Express **25**(23), 28258–28272 (2017).
24. L. Poladian, "Understanding profile-induced group-delay ripple in Bragg gratings," Appl. Opt. **39**(12), 1920–1923 (2000).
25. D. N. Schimpf, E. Seise, T. Eidam, J. Limpert, and A. Tünnermann, "Control of the optical Kerr effect in chirped-pulse-amplification systems using model-based phase shaping," Opt. Lett. **34**(24), 3788–3790 (2009).
26. D. Schimpf, E. Seise, J. Limpert, and A. Tünnermann, "Decrease of pulse-contrast in nonlinear chirped-pulse amplification systems due to high-frequency spectral phase ripples," Opt. Express **16**(12), 8876–8886 (2008).
27. D. N. Schimpf, E. Seise, J. Limpert, and A. Tünnermann, "The impact of spectral modulations on the contrast of pulses of nonlinear chirped-pulse amplification systems," Opt. Express **16**(14), 10664–10674 (2008).
28. S. W. Jolly, N. H. Matlis, F. Ahr, V. Leroux, T. Eichner, A.-L. Calendron, H. Ishizuki, T. Taira, F. X. Kärtner, and A. R. Maier, Spectral phase control of interfering chirped pulses for high-energy narrowband terahertz generation (submitted to) (Nature Photonics.).
29. Y. Hua, G. Chang, F. X. Kärtner, and D. N. Schimpf, "Pre-chirp managed, core-pumped nonlinear PM fiber amplifier delivering sub-100-fs and high energy (10 nJ) pulses with low noise," Opt. Express **26**(5), 6427–6438 (2018).
30. R. W. P. Drever, J. L. Hall, F. V. Kowalski, J. Hough, G. M. Ford, A. J. Munley, and H. Ward, "Laser phase and frequency stabilization using an optical resonator," Appl. Phys. B **31**(2), 97–105 (1983).
31. M. Notcutt, L.-S. Ma, J. Ye, and J. L. Hall, "Simple and compact 1-Hz laser system via an improved mounting configuration of a reference cavity," Opt. Lett. **30**(14), 1815–1817 (2005).
32. C. Grebing, M. Görbe, K. Osvay, and G. Steinmeyer, "Isochronic and isodispersiv carrier-envelope phase-shift compensators," Appl. Phys. B **97**(3), 575–581 (2009).
33. S. Koke, C. Grebing, H. Frei, A. Anderson, A. Assion, and G. Steinmeyer, "Direct frequency comb synthesis with arbitrary offset and shot-noise-limited phase noise," Nature Photonics 4, 462 (2010).
34. E. Lichtman, A. A. Friesem, R. G. Waarts, and H. H. Yaffe, "Stimulated Brillouin scattering excited by two pump waves in single-mode fibers," J. Opt. Soc. Am. B **4**(9), 1397–1403 (1987).
35. W. Liu, D. N. Schimpf, T. Eidam, J. Limpert, A. Tünnermann, F. X. Kärtner, and G. Chang, "Pre-chirp managed nonlinear amplification in fibers delivering 100 W, 60 fs pulses," Opt. Lett. **40**(2), 151–154 (2015).
36. M. Hemmer, G. Cirmi, K. Ravi, F. Reichert, F. Ahr, L. Zapata, O. D. Mücke, A.-L. Calendron, H. Çankaya, D. Schimpf, N. H. Matlis, and F. X. Kärtner, "Cascaded interactions mediated by terahertz radiation," Opt. Express **26**(10), 12536–12546 (2018).
37. S. V. Chernikov and J. R. Taylor, "Measurement of normalization factor of n_2 for random polarization in optical fibers," Opt. Lett. **21**(19), 1559–1561 (1996).